Widely Wavelength-Swept Single-Longitudinal-Mode Fiber Laser With Ultra-Narrow Linewidth in C+L-Band

Da Wei, Ting Feng, *Member, IEEE*, Weiwei Sun, Fengping Yan, and X. Steve Yao, *Fellow, IEEE*

***Abstract*—This study proposes and demonstrates a widely wavelength-swept single-longitudinal-mode (SLM) erbium-doped fiber laser (EDFL) enabled by a dual-coupler-ring based compound-cavity (DCR-CC) filter, a fiber Fabry-Pérot tunable filter (FFP-TF) and a C+L-band erbium-doped fiber amplifier (EDFA). Moreover, it develops a novel methodology utilizing the signal-flow graph combined with the matrix algebra to analyze the DCR-CC filter and obtain its essential design parameters for SLM selection of the EDFL. The C+L-band EDFA is constructed to provide a gain range >90 nm. On the other hand, it demonstrates that, under a sweep-rate ≤100 Hz, a lasing wavelength-swept range >87 nm is obtained, the SLM operation is permanently guaranteed for every instantaneous lasing wavelength. Furthermore, the instantaneous lasing parameters of an optical signal-to-noise ratio ≥66 dB, a relative intensity noise ≤−153.33 dB/Hz@≥3 MHz, a linewidth ≤625 Hz and a power fluctuation ≤0.704 dB are achieved. The distinguished performance of the proposed fiber laser enables it to have a significant potential for application in optical frequency domain reflectometry, spectroscopy and Lidar system.**

***Index Terms*—Fiber laser, wavelength-swept laser, narrow linewidth, compound-cavity filter, signal-flow-graph.**

I. Introduction

With the gradual development and maturity of laser technology, fiber lasers are adopted or anticipated in various optical systems, such as optical communication and spectroscopy [1], fiber Lidar system [2], optical frequency domain reflectometry (OFDR) [3], optical atomic clocks [4], measurements of fundamental constants and physics [5], etc. As the preferred light source in multiple precision measurements and sensing fields, the wavelength-swept fiber laser is promising in terms of wavelength-swept range, instantaneous linewidth and optical signal to noise ratio (OSNR). Furthermore, considering the applications that require a long interference length and narrow linewidth (OFDR, for instance), the wavelength-swept fiber laser is specifically required to operate in single-longitudinal-mode (SLM) to improve the spatial resolution and reduce noise.

Distributed feedback and distributed Bragg reflector (DBR) based ultra-short oscillating cavity structures are effective and practical methods to achieve an SLM operation for fiber lasers. However, most ultra-short cavity fiber lasers produce low output power, have poor characteristics in linewidth and noise, and need additional components to optimize their performance in general [6], [7]. The high-quality long lasing-cavity with an ultra-narrow filter is widely studied due to its flexible structure and distinguished noise characteristics. In this setting, multiple filter structures are able to perform mode selection, such as the superimposed fiber Bragg grating (FBG) [8], silicon-micro-ring-resonator [9], tapered non-adiabatic microfiber based Sagnac mirror [10], polarization-maintaining chirped-Moiré FBG filter [11], short twin-core photonic-crystal-fiber (PCF), based Mach-Zehnder interferometer [12], FBG embedded fiber modal interferometer [13], erbium-doped PCF based equivalent filter [14], etc. However, these filters suffer from their own limitations, such as limited filtering bandwidth, high cost or poor stability. In contrast, compound-cavity fiber filters, composed of several single-coupler-rings and dual-coupler-rings (DCRs), are a group of high-quality filters with ultra-narrow passband, ultra-low cost and ultra-wide operation bandwidth, which enables them to be used for SLM selection of fiber lasers, proved broadly by the studied group and others [15], [23]. Particularly, the DCR-based compound-cavity (DCR-CC) filter proves a favorable performance and application prospect in SLM fiber lasers [22]. Moreover, we have proposed several effective research methodologies to study compound-cavity filters dedicated to SLM fiber lasers [22], [23]. Nevertheless, additional efficient methods are still desired for analyzing various compound-cavity filters. Furthermore, the application potential of the DCR-CC filter in widely wavelength-swept fiber lasers is not verified until present.

Numerous wavelength-tuning methods are proposed in fiber lasers, such as FBG stretching [16], [24], [25], multi-faceted mirror grating rotating [26], acousto-optic modulator [27],

Manuscript received May 29, 2022; accepted June 1, 2022. Date of publication June 8, 2022; date of current version June 17, 2022. This work was supported in part by the National Natural Science Foundation of China under Grants 61975049, 61827818, 61620106014, and 61705057, in part by the Hebei Provincial Natural Science Foundation for Outstanding Young Scholars under Grant F2020201001, in part by the Funding of Hebei 333 Talent Project under Grant A202101010, in part by the Science and Technology Research Project of Colleges and Universities in Hebei Province under Grant ZD2022138, and in part by the Hebei Provincial Innovation Ability Promotion Project under Grant 20542201D. *(Corresponding author: Ting Feng.)*

Da Wei, Ting Feng, Weiwei Sun, and X. Steve Yao are with the Photonics Information Innovation Center, Hebei Provincial Center for Optical Sensing Innovations, College of Physics Science & Technology, Hebei University, Baoding 071002, China (e-mail: weida0328@163.com; wlxyft@hbu.edu.cn; sunweiwei_888@163.com; steveyao888@yahoo.com).

Fengping Yan is with the School of Electronic and Information Engineering, Beijing Jiaotong University, Beijing 100044, China (e-mail: fpyan@bjtu.edu.cn).

Digital Object Identifier 10.1109/JPHOT.2022.3180284

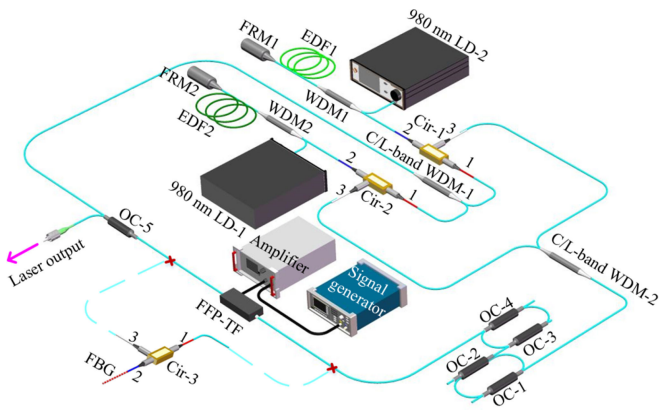

Fig. 1. Schematic diagram of the proposed widely wavelength-swept fiber laser (WWS-EDFL) system.

fiber Fabry-Pérot tunable filter (FFP-TF) [28], [29], etc. In comparison, the FFP-TF presents clear advantages among all-fiber structures such as stable performance, narrow filtering bandwidth, large tuning range, high mechanical stability and long service life. Thus, it is widely used in wavelength-tuning/-sweeping and many other fields. This study proposes and experimentally demonstrates a novel SLM widely wavelength-swept erbium-doped fiber laser (WWS-EDFL), which is mainly enabled by a DCR-CC filter, a C+L-band erbium-doped fiber amplifier (EDFA) and an FFP-TF. Firstly, this study recommends a new theoretical analysis method combing the signal-flow graph with the matrix algebra, which is a general method for studying various complicated compound-cavity filters. This method is used to obtain the significant design parameters for the DCR-CC filter. The C+L-band EDFA is designed to provide a gain range >90 nm, which presents much lower phase-noise and relaxation-noise than the wideband semiconductor optical amplifier. The wavelength-sweeping is achieved by the FFP-TF, driven by a scanning triangular voltage signal. The output performances of swept-range, OSNR, stability and linewidth are characterized in detail in the following sections.

II. Experimental Setup, Principle and Theory

A. Fiber Laser Configuration and Analysis

The diagram of the proposed WWS-EDFL is shown in Fig. 1. The lasing gain part is a C+L-band EDFA, composed of a C-band EDFA and an L-band EDFA in parallel, through two C/L-band wavelength-division-multiplexers (WDMs, WDM-1 and WDM-2). The C-band EDFA and L-band EDFA contain a 2 m long erbium-doped fiber (EDF) (EDF1, Fibercore, M12-980-125) and a ∼9 m long EDF (EDF2, LIEKKI^{TM} Er80-8-125) as the gain medium, respectively. Each EDF is pumped by a 980 nm laser diode (LD, LD-1 or LD-2) through a 980/1550 nm WDM (WDM1 or WDM2). Two EDFAs adopt each a special structure containing a circulator (Cir1 or Cir2) and a Faraday rotation mirror (FRM1 or FRM2), due to which the small laser signal is amplified twice after being reflected by the FRMs to use the gain ions of EDFs sufficiently. This is not only beneficial for suppressing the high spontaneous emission noise but also helps to improve the pump laser utilization. Furthermore, the FRMs avoid the formation of spatial hole burning in the EDFs. In the C-band EDFA, a 7 m long single-mode fiber (SMF) is inserted to assure a similar light path length to the L-band EDFA. This means the C-band and L-band EDFAs are with symmetric structures in the laser cavity to guarantee fine switching between two EDFAs during wavelength-sweeping. An FFP-TF (Micron Optics Cor., FFP-TF2) with a 3 dB passband (full-width at half-maximum, FWHM) of 0.14 nm (corresponding to a frequency bandwidth of ∼17.5 GHz) and a fineness of 659 is employed as the wavelength defining element. It is driven by a signal generator (Tektronix, AFG3232C) through a power amplifier (Aigtek, ATA-2021H). A DCR-CC filter, assembled using four optical couplers (OC-1, OC-2, OC-3, and OC-4) and having precisely designed fabrication parameters, is used as a narrow passband comb filter to select only one longitudinal mode among the dense modes of the main-ring cavity (MRC), assisted by the FFP-TF. The FFP-TF part between two marked points, as shown in the figure is replaced by a uniform FBG with a reflection bandwidth approximately equal to the passband of the FFP-TP, with the assistance of another circulator (Cir-3), to obtain the fixed single-wavelength operation for further performance research. The length of the MRC is approximately 26.20 m, indicating that the longitudinal mode spacing is ∼7.80 MHz. The laser is extracted from the 10% port of another coupler (OC-5) for measurement.

B. Theory of the DCR-CC Filter

As described in [23], [30], [31], the signal-flow-graph helps understand the compound-cavity filter system operation, using a pictorial representation, and to easily conclude the causal relationship between optical signal transformation and transmission. Compared with the multi-beam interference method, the signal-flow-graph considers a compound-cavity filter as a linear system, which allows the filter to be solved by the algebraic equation, similarly to the analysis of micro-ring resonators in dense WDM systems [32], [33]. However, it is difficult to analyze the complicated compound-cavity filter structure by solving the algebraic equation. The advantage presented by the signal-flow-graph is using the node, instead of each sub-cavity, as the smallest unit to analyze, avoiding considering the most difficult energy and signal interleaving between sub-cavities. That enables the introduction of the simple numerical method-based matrix algebra [34] to obtain the input-output relationship of the filter under research. Therefore, this study uses the signal-flow-graph to analyze the DCR-CC filter system and the matrix algebra to solve the node-relationship.

The schematic diagram of the DCR-CC filter is shown in Fig. 2(a). It is composed of two cascaded DCRs. Each DCR is composed of two 2 × 2 fiber OCs. 1-16 and E1-E16 are respectively set as the light ports of 4 OCs and the corresponding electric-field amplitudes. The signal-flow-graph of DCR-1 is shown in Fig. 2(b). Ports 1-8 are represented by 8 photonics nodes. The straight transmittance C_i of OCs is defined as

$$C_i = \sqrt{1-\gamma_i}\sqrt{1-\kappa_i}\,(i = 1, 2, 3, 4)\,. \tag{1}$$

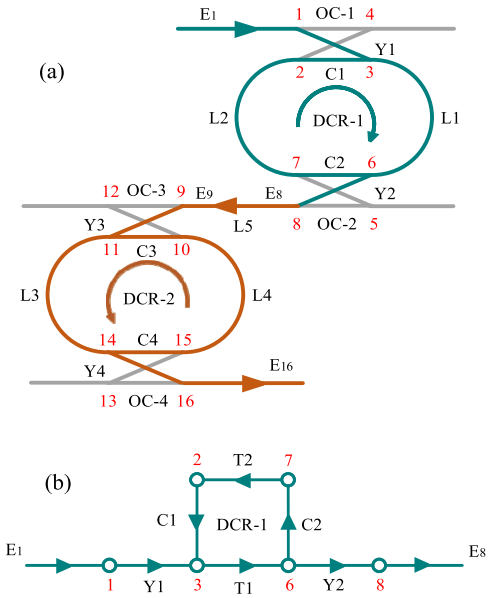

Fig. 2. (a) Schematic diagram of DCR-CC filter. (b) Signal-flow-graph of DCR-1.

The cross-coupling transmittance Y_i of OCs is as follows

$$Y_i = j\sqrt{\kappa_i}\sqrt{1-\gamma_i}\,(i=1,2,3,4)\,. \tag{2}$$

The propagating gain T_i of fiber optical paths is as follows

$$T_i = \sqrt{1-\delta}e^{(-\alpha+j\beta)L_i}\,(i=1,2,3,4)\,, \tag{3}$$

where L_i is the length of the i-th fiber, κ_i $(i=1,2,3,4)$ and γ_i $(i=1,2,3,4)$ are the coupling ratio and insertion loss of the i-th OC respectively, α is the fiber loss coefficient, δ is the fusion splicing loss, $\beta = 2\pi n_{eff}/\lambda$ is the light propagation constant, n_{eff} is the effective refractive index, λ is the light wavelength and j is the imaginary part. The inflow and outflow relationships of the optical signal between neighboring nodes are represented by a set of inhomogeneous linear equations, as expressed in (4), where $E1$ is equal to 1 and $E5$ is equal to 0.

$$\begin{cases} E_1 = 1 \\ E_2 = T_2E_7 \\ E_3 = Y_1E_1 + C_1E_2 \\ E_4 = C_1E_1 + Y_1E_2 \\ E_5 = 0 \\ E_6 = T_1E_3 \\ E_7 = Y_2E_5 + C_2E_6 \\ E_8 = C_2E_5 + Y_2E_6 \end{cases}. \tag{4}$$

Generally, the transmission relation of DCR-1 between the input and output is derived from (4) directly, as

$$\frac{E_8}{E_1} = \frac{-\sqrt{1-\gamma_1}\sqrt{1-\gamma_2}\sqrt{1-\delta}\sqrt{\kappa_1}\sqrt{\kappa_2}e^{(-\alpha+j\beta)L_1}}{1-\sqrt{1-\gamma_1}\sqrt{1-\gamma_2}\sqrt{1-\kappa_1}\sqrt{1-\kappa_2}(1-\delta)e^{(-\alpha+j\beta)(L_1+L_2)}}. \tag{5}$$

It is clear that (5) is identical to the analytical solution acquired by another method proposed in previous work [22]. However, it is difficult to obtain an analytical solution for the transmission relation of a compound-cavity filter having a complicated structure with numerous photonics nodes. Fortunately, matrix algebra is used to acquire the numerical solution directly. Hence, the (4) is modified as

$$\begin{cases} E_1 = 1 \\ -E_2 + T_2E_7 = 0 \\ Y_1E_1 + C_1E_2 - E_3 = 0 \\ C_1E_1 + Y_1E_2 - E_4 = 0 \\ E_5 = 0 \\ T_1E_3 - E_6 = 0 \\ Y_2E_5 + C_2E_6 - E_7 = 0 \\ C_2E_5 + Y_2E_6 - E_8 = 0 \end{cases}. \tag{6}$$

Three matrices are decomposed from Eq. (6), which are the coefficient matrix $\mathbf{M}$, the output field matrix $\mathbf{E_{out}}$ and the input or initial field matrix $\mathbf{E_{in}}$. Thus, the following equation is obtained

$$\mathbf{M}\mathbf{E_{out}} = \mathbf{E_{in}}. \tag{7}$$

The matrices' elements are expressed as

$$\mathbf{M} = \begin{bmatrix} 1 & 0 & 0 & 0 & 0 & 0 & 0 & 0 \\ 0 & -1 & 0 & 0 & 0 & 0 & T_2 & 0 \\ Y_1 & C_1 & -1 & 0 & 0 & 0 & 0 & 0 \\ C_1 & Y_1 & 0 & -1 & 0 & 0 & 0 & 0 \\ 0 & 0 & 0 & 0 & 1 & 0 & 0 & 0 \\ 0 & 0 & T_1 & 0 & 0 & -1 & 0 & 0 \\ 0 & 0 & 0 & 0 & Y_2 & C_2 & -1 & 0 \\ 0 & 0 & 0 & 0 & C_2 & Y_2 & 0 & -1 \end{bmatrix}, \mathbf{E_{out}} = \begin{bmatrix} E_1 \\ E_2 \\ E_3 \\ E_4 \\ E_5 \\ E_6 \\ E_7 \\ E_8 \end{bmatrix},$$

$$\mathbf{E_{in}} = \begin{bmatrix} 1 \\ 0 \\ 0 \\ 0 \\ 0 \\ 0 \\ 0 \\ 0 \end{bmatrix} \tag{8}$$

Then the $\mathbf{E_{out}}$ is directly solved numerically as

$$\mathbf{E_{out}} = \mathbf{M}^{-1}\mathbf{E_{in}}. \tag{9}$$

Similarly, the E_8 of DCR-1 and E_{16} of DCR-2 are acquired, respectively. Moreover, the transmittance of the DCR-CC filter is expressed as

$$T_{out} = (E_8 \cdot T_5 \cdot E_{16}) \cdot (E_8 \cdot T_5 \cdot E_{16})^*. \tag{10}$$

In the WWS-EDFL, the FFP-TF is used as a wavelength-defining and sweeping device. Since the FFP-TF, as well as the DCR-CC filter, are corporately used to select the SLM in the laser cavity, the free spectrum range (FSR) of the DCR-CC should be 0.5-1 times the FFP-TF's FWHM. Secondly, in order to select one expected mode from the dense longitudinal modes of the MRC, the longitudinal mode spacing should also be 0.5-1 times the DCR-CC's transmission FWHM. When the

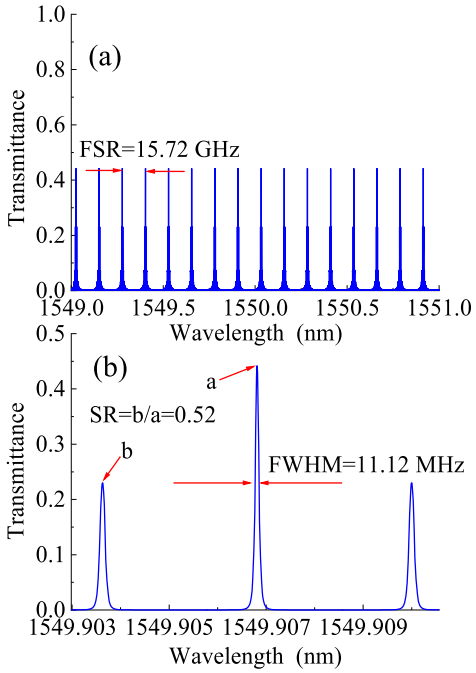

Fig. 3. (a) Simulated transmission spectrum of DCR-CC filter. (b) Details of a certain transmission channel.

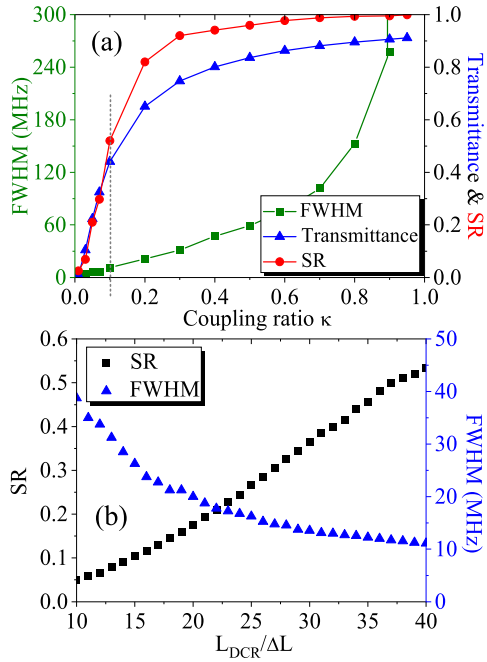

Fig. 4. Design curves of the DCR-CC filter. (a) Variations of FWHM, transmittance and SR with changing of coupling ratio κ of four OCs used. (b) Variations of SR and FWHM with changing of $L_{\mathrm{DCR}-1}/\Delta L$.

above-mentioned two aspects are satisfied, only one longitudinal mode lasing exists continuously in the cavity, regardless of the wavelength-sweeping or fixed-wavelength operation mode. Therefore, the FSR of the DCR-CC should be 8.75−17.50 GHz according to the FFP-TF's transmission FWHM of 17.50 GHz. The DCR-CC's FSR is calculated as

$$\mathrm{FSR} = \frac{c}{n_{eff}\Delta L}, \tag{11}$$

where c is the speed of light in vacuum, and ΔL is the cavity length difference between the DCR-1 and DCR-2. Furthermore, the DCR-CC's transmission FWHM should be ∼7.80−15.60 MHz according to the MRC's longitudinal mode spacing of ∼7.80 MHz. The final specially designed transmission response of the DCR-CC simulated is shown in Fig. 3. As shown in Fig. 3(a) and 3(b), the FSR of the designed DCR-CC filter is 15.72 GHz with a transmission FWHM of 11.12 MHz, which conforms to the aforementioned expected parameter requirement, and the suppression ratio (SR) is 0.52, indicating an adequate filtering effect. The simulation parameters used are $\kappa =$ 0.1, $\Delta L = 1.30$ cm, DCR-1's and DCR-2's lengths of 50.70 cm and 52.00 cm respectively, $\alpha = 0.2$ dB/km, $\delta = 0.01$ dB, γ_i $(\mathrm{i} = 1, 2, 3, 4) = 0.09$ dB, and $n_{eff} = 1.468$.

The above-mentioned parameter design process is almost similar to that in [22]. Firstly, according to the handwork tolerance and operation error of fiber splicing and (11), it is imperative to start by determining a ΔL(1.3 cm) for the DCR-CC filter. Afterward, the cavity lengths ($L_{\mathrm{DCR}-1}$ and $L_{\mathrm{DCR}-2}$) of the DCR-1 and DCR-2 should be both the integer multiple of ΔL to obtain the optimal flatness of the transmission envelope and the smallest SR for the DCR-CC filter [35]. Under the determination of $L_{\mathrm{DCR}-1} = 50.70$ cm and $L_{\mathrm{DCR}-2} = 52.00$ cm, the design curves of the DCR-CC filter are given in Fig. 4(a), where it is clear that the FWHM, transmittance and SR of the DCR-CC filter are dependent on one another with the changing of the coupling ratio κ of four OCs. The $\kappa = 0.1$ for four OCs is determined after considering a tradeoff among three parameters. Furthermore, with $\kappa = 0.1$, the SR and FWHM of the DCR-CC filter versus the ratio of $L_{\mathrm{DCR}-1}/\Delta L$ which is given as integers, as shown in Fig. 4(b), are studied. The two curves exhibit that the ratio $L_{\mathrm{DCR}-1}/\Delta L$ (50.70/1.30 = 39) which is chosen for the DCR-CC design is reasonable.

III. Experimental Results and Discussion

A. Measurement of the DCR-CC

According to the acquired parameters, the DCR-CC filter is fabricated, and its transmission spectrum measured using the measurement system, which is described in a previous work [22]. As shown in Fig. 5(a), the FSR is 15.78 GHz, which is consistent with that obtained in the simulated transmission spectrum. The minor transmittance discrepancy among different transmission channels is caused mainly by the handwork induced error for cavity length difference ΔL and the minor deviations of four OCs' coupling-ratios κ from the designed value of 0.1. Fig. 5(b) shows a typical transmission channel of a DCR-CC filter, and the measured SR is 0.63. The FWHM of the main channel is 12.51 MHz, as shown in inset-1, which guarantees that a SLM is able to pass through it. Note that the slight fluctuation presented in the curve in inset-1, is caused by the minor frequency jitter and scanning nonlinearity of the tunable laser source.

To verify the ultra-wide working band of the DCR-CC filter, this study measured its transmission spectra at the wavelength

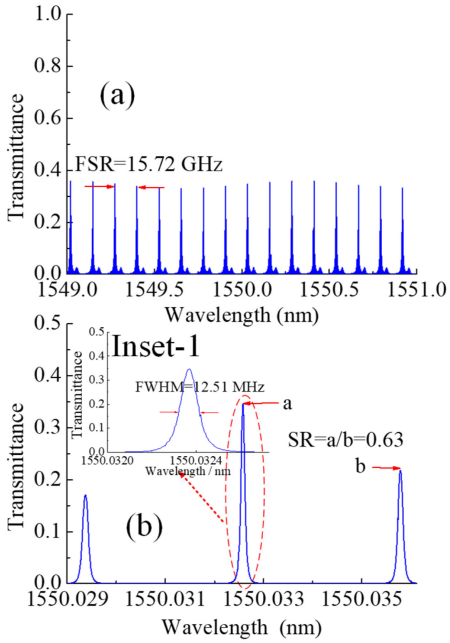

Fig. 5. (a) Measured transmission spectrum of the DCR-CC filter. (b) Zoomed-in one typical transmission channel; inset-1 showing details of the main transmission channel.

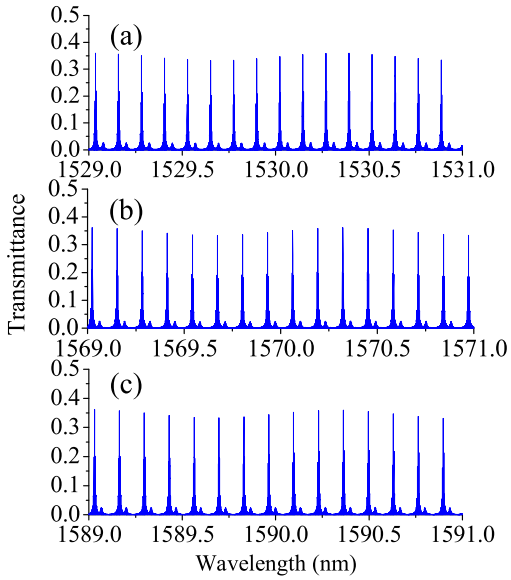

Fig. 6. Measured transmission spectra of DCR-CC filter around wavelengths of (a) 1530 nm, (b) 1570 nm and (c) 1590 nm, respectively.

regions around 1530 nm, 1570 nm and 1590 nm respectively, as shown in Fig. 6(a) to (c). It is clear that the filtering characteristics in all three wavelength regions are similar to that around 1550 nm. Minor differences in the FSR and FWHM in different wavelength regions are mainly due to the variations of wavelength-dependent parameters of OCs and the chromatic dispersion of the silica SMF used.

B. Performance in Wavelength-Swept Lasing Mode

The amplified spontaneous emission (ASE) spectrum of the C+L-band EDFA and the possible laser wavelength-tuning

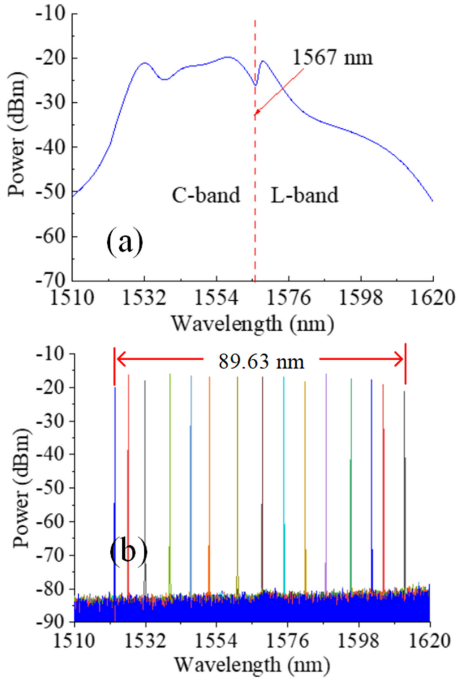

Fig. 7. (a) Amplified spontaneous emission spectrum of the C+L-band EDFA. (b) Tunable range of the WWS-EDFL.

range of the WWS-EDFL are firstly investigated using an optical spectrum analyzer (OSA, Yokogawa AQ6370D) with a resolution of 0.02 nm and a data sampling interval of 0.001 nm. By adjusting the two 980 nm pump lasers' powers to suitable values, the ASE of the EDFA at the position behind the C/L-WDM2 is measured, as shown in Fig. 7(a), which covers the whole C+L-band with a wavelength range of almost 90 nm. Note that the abnormal notch at ~1567 nm is caused by the inherent 3 dB loss of the C/L-WDMs at the splitting wavelength. In order to find the lasing wavelength range of the WWS-EDFL, the FFP-TF2's driving voltage is tuned from 1.2 V to 23.6 V to observe the lasing output of the fiber laser. The largest tunable range obtained is 89.630 nm, from 1522.520 nm to 1612.150 nm, as shown in Fig. 7(b).

Afterward, the characteristics of wavelength-swept mode of the WWS-EDFL are studied under different sweep rates. The driving signal of the FFP-TF2 is a triangular voltage with a tunable sweep rate (10 Hz, 50 Hz, 100 Hz and 150 Hz) and an offset voltage of 24.40 V. The peak-to-peak voltage is 24.86 V when the sweep rate is equal to 10 Hz. As the sweep rate increases, the peak-to-peak voltage eventually increases to 27.43 V. Note that since the WWS-EDFL might generate strong Q-switched pulses in the process of wavelength-sweeping due to the nonlinear Kerr effect [27] - which may damage the fiber-endface reflective coatings of Fabry-Pérot cavity of the FFP-TF - the pump power at a suitable level of ~200 mW is controlled and the DCR-CC filter is placed in front of the FFP-TF2 for additional protection. Using the maximum-hold (MH) mode of OSA and after repeatedly scanning the spectrum, the wavelength-swept ranges are measured for four sweep rates respectively, as shown in Fig. 8(a) to (d), where it is clear that the entire wavelength sweep ranges are larger than 85 nm for all four sweep rates.

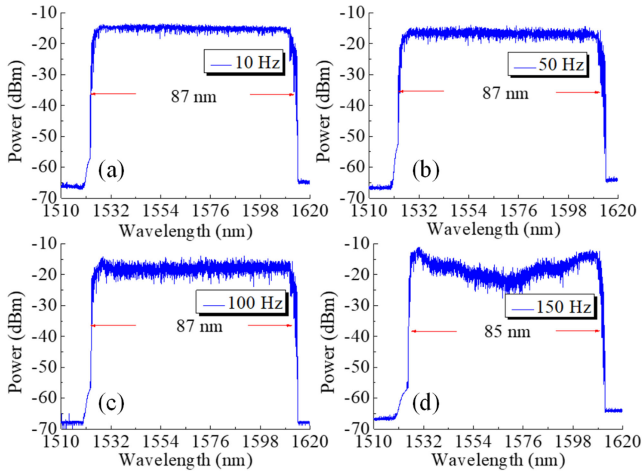

Fig. 8. Typical laser spectra when voltages applied on FFP-TF2 with sweep rates of (a) 10 Hz, (b) 50 Hz, (c) 100 Hz, and (d) 150 Hz, respectively.

Moreover, the power of the laser spectrum in the middle part decreases with the increase of the sweep rate. This phenomenon is due to two reasons. First of all, when working at a high driving frequency, the response of the piezoelectric-transducer (PZT) assembled in the FFP-TF is not perfect at the turning points of the triangle-wave driving signal. Subsequently, the wavelength-sweeping speed around the turning points, corresponding to both sides of the spectrum, is obviously lower than that in the middle linear region of the driving signal, corresponding to the spectral middle part. However, the OSA requires a sufficient integral time to acquire every data point when functioning with a given high resolution. Therefore, when the dwell time of a transient lasing mode is less than that measurement integral time, the measured spectral power level is negatively correlated with the instantaneous wavelength-sweeping speed and hence, the middle part of the spectrum is inferior to its both sides. The second reason is that the longitudinal mode of the proposed WWS-EDFL may not be stable enough in the high-speed wavelength-swept mode. This is induced mainly by the limitation of the laser establishing time for a certain longitudinal mode, which is subject to further explanation, subsequently.

To verify the SLM operation of the WWS-EDFL in wavelength-swept mode, the self-homodyne method with a 400 MHz photodetector (PD, Thorlabs PDB470C) and a radio frequency (RF) electrical spectrum analyzer (ESA, Keysight N9010A) is used for measurement. The RF noise spectra over 0−400 MHz are measured under four sweep rates with a resolution bandwidth (RBW) of 51 kHz, as shown in Fig. 9. As seen in Fig. 9(a) to (d), when the sweep rate is inferior to 150 Hz, no obvious beating signal is captured, indicating that the laser maintains the instantaneous SLM operation in the wavelength-swept mode. On the contrary, when measuring via the MH mode of ESA, the beating noise is higher than that measured in the corresponding single-scanning mode of the ESA for each sweeping rate, as shown in Fig. 9(e) to (h), respectively. It is believed that the captured higher noise is mainly due to the extremely fast mode-switching from an unstable mode to another one. In particular, for the sweeping rate of 150 Hz, as shown in Fig. 9(h), a clear noise is captured in the MH mode, indicating that the WWS-EDFL is unable to obtain enough stable instantaneous longitudinal-mode lasing under a sweeping rate larger than 150 Hz.

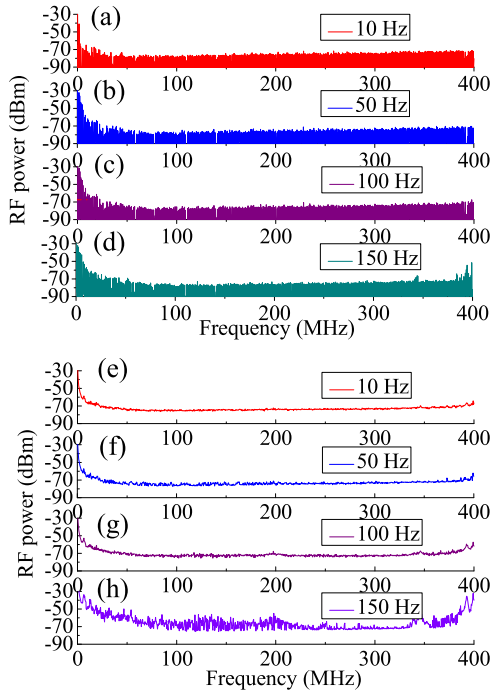

Fig. 9. RF beating spectra measured by self-homodyne system in swept mode of WWS-EDFL with a triangular driving voltage for FFP-TF2 at sweeping rates of (a) 10 Hz, (b) 50 Hz, (c) 100 Hz and (d) 150 Hz respectively using ESA's single-scanning mode, and at sweeping rates of (e) 10 Hz, (f) 50 Hz, (g) 100 Hz and (h) 150 Hz respectively using ESA's maximum-hold (MH) mode.

C. *Performance in Fixed Wavelength Lasing Mode*

Although several effective techniques are proposed and demonstrated to measure the instantaneous spectrum of swept lasers [36]–[39], they all suffer from various limitations and are not able to directly measure the instantaneous laser linewidth as narrow as $<$10 kHz of an SLM WWS-EDFL with a sweeping range $>$80 nm. Furthermore, the creep effect of the PZT-based FFP-TF induces the lasing wavelength unstable, even when using a constant driving voltage for the FFP-TF. Therefore, this study proposes an indirect method to characterize the laser output quality of the WWS-EDFL by further using four FBGs with different center wavelengths of 1530 nm, 1550 nm, 1570 nm and 1590 nm in turn, with the assistance of a circulator to replace the FFP-TF, as shown in Fig. 1. All FWHMs of four FBGs are close to that of the FFP-TFs. Using the four FBGs in turn, the output laser spectra are measured as shown in Fig. 10(a) to (d). In each figure, the measurement is performed by repeatedly scanning the OSA with a time interval of 4 min. The measured lasing wavelengths are centered at $\lambda 1 = 1530.0223$ nm, $\lambda 2 = 1550.0587$ nm, $\lambda 3 = 1569.9302$ nm and $\lambda 4 = 1590.0985$ nm, respectively. The OSNRs are all $>$66 dB. Almost no wavelength fluctuation exists for all four lasers, and the maximum fλi ($i =$

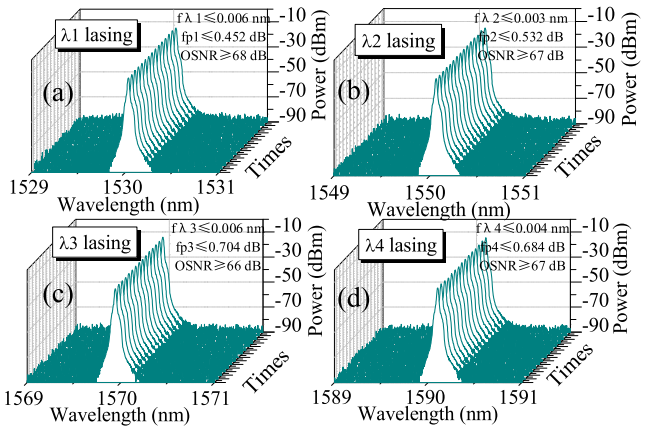

Fig. 10. Laser spectra after replacing FFP-TF2 with FBG and circulator, with FBG's reflection center wavelength of (a) ∼1530 nm (b) ∼1550 nm, (c) ∼1570 nm and (d) ∼1590 nm respectively, under a measurement time of 60 min. fλ*i* ($i = 12,34$): wavelength fluctuation of λ*i*; fp*i* ($i = 12,34$): power fluctuation of λ*i*; OSNR: optical signal-to-noise ratio; in each figure, 15 repeated OSA's scans measured with a time interval of 4 min.

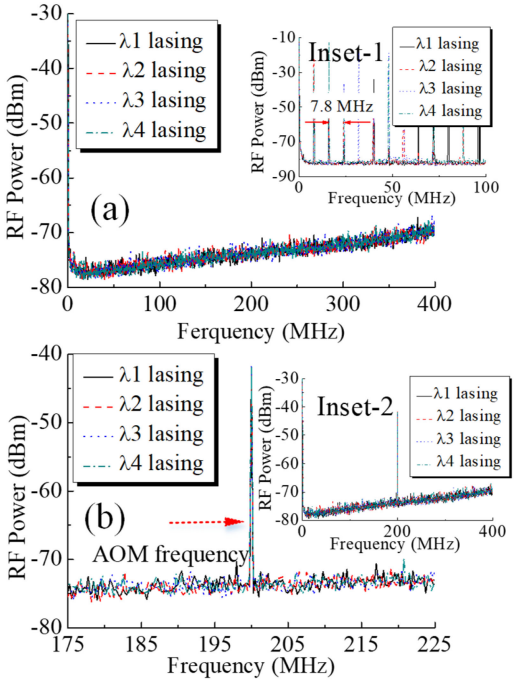

Fig. 11. RF spectra of four lasers measured by ESA. (a) Self-homodyne RF spectra measured in a range of 0-400 MHz using MH mode of ESA in ∼10 min with RBW of 51 kHz; Inset-1 showing the similar RF spectra after the DCR-CC replaced by SMF, measured in 0-100 MHz. (b) Delayed self-heterodyne measurement RF spectra measured in a range of 175-225 MHz using MH mode of ESA in ∼20 min with RBW of 51 kHz; inset-2 showing similar RF spectra measured in 0-250 MHz in ∼30 min with RBW of 30 kHz.

1, 2, 3, 4) is only 0.006 nm, less than the resolution of the OSA. Moreover, the maximum fp*i* ($i = 12,34$) is ≤0.704 dB.

Using the self-homodyne method again, the SLM characteristics of four lasers are measured, as shown in Fig. 11(a). Using the MH mode in a ∼10 min measurement, no beating signal is captured for all four lasers, which means that the EDFL is working properly in SLM lasing. Using a section of SMF to replace the DCR-CC filter to ensure that the MRC's length is

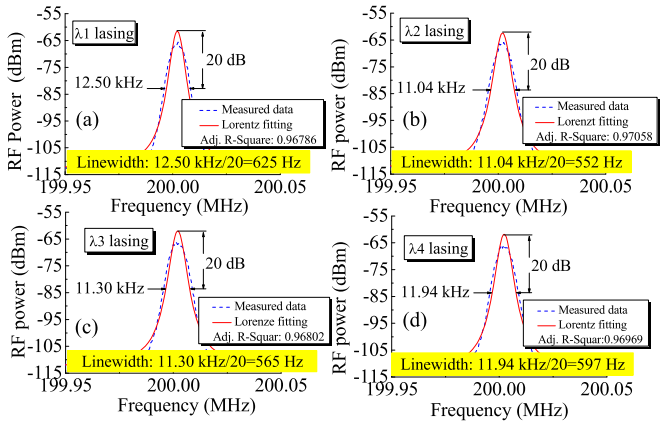

Fig. 12. Linewidths measured by the DSHM system for four lasers at (a) λ1, (b) λ2, (c) λ3 and (d) λ4, respectively. ESA's average mode used to scan 100 times in the range of 199.950−200.050 MHz with a RBW of 100 Hz. Lorentz fitting implemented to each spectrum.

unchanged, the RF beat spectra of four lasers are measured again, as shown in the inset-1 of Fig. 11(a). It is clear that multiple beating frequency signals are captured, indicating that all the lasers are functioning in a dense multi-longitudinal mode lasing. That verifies the capability of SLM selection of the DCR-CC filter in the fiber laser. As shown in inset-1, the spacing of adjacent peaks is ∼7.80 MHz, corresponding to a MRC's length of ∼26.19 m, which is consistent with the measured length of ∼26.20 m of MRC. Note that the noise level increases along with the frequency in Fig. 11(a) due to the inherent property of the PD.

The mode-hop characteristics of four lasers are studied using a delayed self-heterodyne measurement (DSHM) system, which is composed of a 400 MHz PD, a Mach-Zehnder interferometer (MZI) and an ESA. On the other hand, the MZI is composed of a 200 MHz acousto-optic modulator (AOM) in one arm and a 100 km long SMF in the other. Using ESA's MH mode for ∼20 min measurement, the beating spectra are shown in Fig. 11(b) in a frequency range of 175−225 MHz with an RBW of 30 kHz. Moreover, Inset-2 presents the measurement results in the frequency range of 0−250 MHz with an RBW of 51 kHz. It is clear that only the 200 MHz strong beat frequency signal introduced by the AOM is captured for each laser measurement. Considering that the longitudinal mode interval of the MRC is ∼7.80 MHz, it is believed that the fiber laser functions in a stable SLM without mode-hop for a significant period of time.

Furthermore, the linewidths of four lasers are studied via the DSHM system. For each measurement, 100 times scans are repeated using the average mode of ESA. Fig. 12(a) to (d) show the measured RF beat spectra of the four lasers, respectively. The Lorentz fitting is implemented to each measured spectrum, and the Adj. R-Square values are 0.96786, 0.97058, 0.96802 and 0.96969, respectively. As shown in the four figures, by calculating the 1/20 of 20-dB bandwidth of the fitted curves, the linewidths of four single-wavelength lasers are 625 Hz, 552 Hz, 565 Hz and 597 Hz, respectively. Note that the 100 km SMF in the DSHM provides a measurement resolution of 2 kHz, so the 20-dB bandwidths reading out from four figures are accurate.

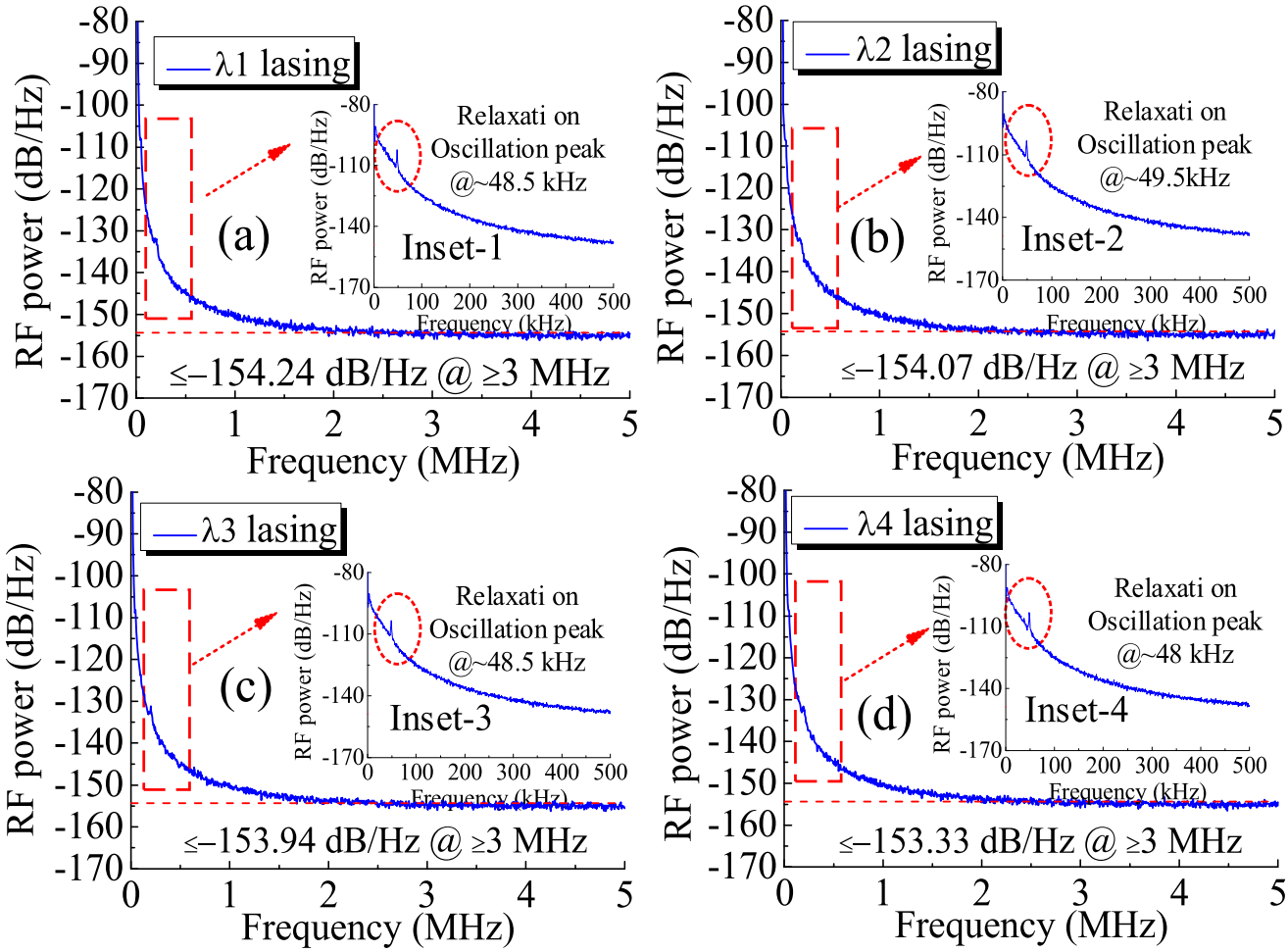

Fig. 13. RINs measured for four lasers at (a) λ1, (b) λ2, (c) λ3 and (d) λ4, respectively, in 0−5 MHz with RBW of 10 kHz for ESA. Inset-1 to inset-4 show the similar measurements in 0-500 kHz with RBW of 100 Hz.

However, in theory, the longer difference between the lengths of MZI's two arms is adopted, and the closer measurement result of the true linewidth of a laser is obtained from the DSHM system. However, a too long SMF delay will introduce a strong 1/*f* noise, which will cause the measurement linewidth to widen from the Lorentz type to the Gauss type [21]. Considering that a high R-Square value is obtained for each curve fitting, it is believed that the measured linewidths can be used as the natural conservative linewidths of four lasers.

The relative intensity noise (RIN) of each lasing wavelength is measured via the 400 MHz PD, an oscilloscope (Tektronix, TDS2024C) and the ESA. The oscilloscope is used to measure the DC signal output voltage of the PD to calculate the power in the ESA, while the ESA is used to measure the power spectral density of the PD output. As shown in Fig. 13(a) to (d), the RINs for fours lasers are all lower than −153 dB/Hz when the frequency is ≥3 MHz. From inset-1 to inset-4 of Fig. 13, the relaxation oscillation peaks are all close to 48.50 kHz, while all the peak values of four lasers are ≤−100 dB/Hz. The position of the relaxation oscillation peak is mainly induced by the cavity length, while the relaxation oscillation noise is mainly induced by the combining influences, including the pump power, cavity loss, mechanical vibration and thermal disturbance [40]. As the cavity length increases, the position of the relaxation oscillation peak moves in a descending frequency direction.

D. Performance Analysis of Wavelength-Swept Mode

This section theoretically verifies that the performance of the proposed WWS-EDFL in the wavelength-swept mode under a given sweep rate is comparable with that in the fixed lasing wavelength mode, characterized above. According to the laser principle, it is known that a small light signal needs time to propagate enough loops and obtain enough gain in the laser cavity, in order to become a stable laser. This indicates that for a wavelength-swept fiber laser enabled by an FFP-TF, the passband of the scanning filter must remain for a sufficient period τ_{mode} to make any single lasing mode oscillate. In that situation, the instantaneous lasing property is almost similar to that in the fixed lasing wavelength mode. In other words, if the sweep rate is extremely large, the instantaneous lasing property is degraded due to insufficient oscillation. For the suggested WWS-EDFL, the wavelength-swept range of 87 nm contains 691 transmission channels of the DCR-CC filter. Subsequently, in each sweep period, the passband of the FFP-TF is able to scan over 1382 lasing modes. Therefore, to obtain sufficient oscillation for each

mode, the following relationship must be satisfied.

$$\tau_{\text{mode}} = \frac{1}{1382 \times f}, \tag{13}$$

where f is the sweep rate of the FFP-TF. For the typical sweep rates of 10 Hz, 50 Hz, 100 Hz and 150 Hz used in experiments, the corresponding τ_{mode} calculated are 72.3585 μs, 14.4717 μs, 7.2358 μs and 4.8239 μs, respectively.

The necessary cycle number for a cavity mode to form a stable laser oscillation is determined by the net gain of open loop G_{net}, which is expressed as

$$G_{\text{net}} = G_{\text{EDFA}} - A_{\text{filter}} - A_{\text{other}} - A_{\text{OC}}, \tag{14}$$

where G_{EDFA} is the gain of the EDFA, A_{filter} denotes the insertion loss of the FFP-TF, A_{other} denotes the attenuation introduced by other passive devices and loss of fiber pigtails in the laser cavity, and A_{OC} is the loss induced by the output coupling ratio of OC-5. According to the estimation and measurement, the G_{EDFA}, A_{filter}, A_{other} and A_{OC} are ~20 dB, 4.56 dB, ~5 dB and 0.46 dB, respectively. Therefore, the G_{net} is calculated to be equal to 10 dB approximately. According to the measured output OSNR of ~67 dB for the proposed fiber laser, as shown in Fig. 10, the OSNR should be about 77 dB considering the 10% output ratio of OC-5. Consequently, a certain longitudinal mode must oscillate 8 loops to be considered a stable laser. However, given the gain saturation effect presented in the EDF, the required cycle number should be larger than 8 loops, while 15 loops should be sufficient for achieving a high-performance laser. Furthermore, the DCR-CC filter is a ring oscillating cavity device. Thus, the desired filtering effect is obtained based on a sufficient light oscillation in the two subring cavities. Based on the analysis method suggested in previous work [22], the transmittance $T_{\text{DCR}-1}$ is expressed as

$$\begin{aligned} T_{\text{DCR}-1} &= \left(\frac{E_8}{E_1}\right)\left(\frac{E_8}{E_1}\right)^* \\ &= \left[Y_1L_1Y_2 + \sum_{N=1}^{\infty} Y_1L_1Y_2 \cdot (C_1L_1C_2L_2)^N\right] \\ &\quad \times \left[Y_1L_1Y_2 + \sum_{N=1}^{\infty} Y_1L_1Y_2 \cdot (C_1L_1C_2L_2)^N\right]^*, \end{aligned} \tag{15}$$

where N is the cycle number of lights inside the ring oscillating cavity. Using the parameters given in Section II.B, the transmittance spectra of DCR-1 under different cycle numbers are calculated as shown in Fig. 14(a). Similarly, the transmittance spectra of DCR-2 are theoretically obtained, as shown in Fig. 14(b). Hence, for two subrings, when both their cycle numbers are superior to 40, the transmittance and passband are stabilized.

According to the previous analysis, in order to achieve stable lasing, a longitudinal mode in the laser cavity needs at least a time τ to oscillate, where τ is expressed as

$$\tau = \frac{N_{\text{loops}} \cdot n_{\text{eff}} \cdot [L_{\text{MCR}} + (L_{\text{DCR}-1} + L_{\text{DCR}-2}) \cdot N_{\text{filter}}]}{c}, \tag{16}$$

where, $N_{\text{loops}} = 15$ and $N_{\text{filter}} = 40$, respectively, denote the cycle numbers of light necessary in the active main ring cavity

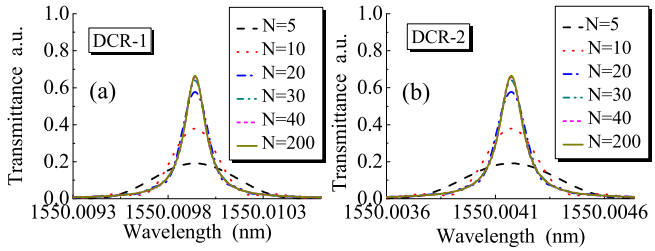

Fig. 14. Simulated transmission spectra of (a) DCR-1 and (b) DCR-2, under different cycle numbers of lights inside the subrings.

(MCR), and two passive subrings, $L_{\text{MCR}} = 26.20$m, $L_{\text{DCR}-1} = 50.70$ cm and $L_{\text{DCR}-2} = 52.00$ cm represent the lengths of the MCR and two subrings and c is the light speed in a vacuum, respectively. Therefore, a minimum time $\tau$of a stable laser established in the laser cavity is calculated to be 4.9383 μs. Compared with the τ_{mode} for four typical sweep rates, only for the sweep rate of 150 Hz, the τ_{mode} is inferior to the τ, in which the instantaneous lasing mode is unable to oscillate sufficiently. That is exactly consistent with the result acquired and analyzed in the experiment shown in Fig. 9(d). Therefore, it is concluded that, conservatively under a sweep rate $\leq$100 Hz for the WWS-EDFL, the instantaneous lasing performance in the wavelength-swept mode is similar to that in the fixed wavelength lasing mode.

IV. Conclusion

This paper reports a WWS-EDFL enabled by a DCR-CC filter, an FFP-TF, and a C+L-band EDFA. A novel methodology that utilizes signal-flow-graph combined with matrix algebra to obtain the significant design parameters of the DCR-CC is introduced. This can be a general method to analyze the compound-cavity filter used for mode selection in fiber lasers. Furthermore, this study designed and fabricated the DCR-CC filter with an FSR of 15.78 GHz and an FWHM of 12.51 MHz. The C+L-band EDFA is established to reach a wavelength-swept range >87 nm. Theoretically, this paper verified that under a sweep rate <100 Hz, the proposed WWS-EDFL possesses the output performance in any instantaneous lasing wavelength comparable with that in the corresponding fixed wavelength lasing mode. Four typical FBGs with the center reflection wavelengths of 1530 nm, 1550 nm, 1570 nm and 1590 nm, respectively, are used to replace the FFP-TF for wavelength defining. Afterward, the corresponding fixed single-wavelength operations are characterized in turn. All lasers have an OSNR $\geq$66 dB, a RIN ≤ -153.33 dB/Hz@$\geq$3 MHz, and a linewidth $\leq$625 Hz. Furthermore, the power fluctuation is $\leq$0.704 dB, and no mode-hopping is observed within 20 min for all lasers. The obtained performance parameters for fixed wavelength lasing are considered as an estimation for those of the proposed WWS-EDFL under a sweep-rate $\leq$100 Hz. Moreover, the laser output power in swept-mode is easily further amplified using an extra EDFA for high power application requirements. It is believed that, if with specialized temperature compensation and vibration isolation, the proposed WWS-EDFL can be as an ideal alternative laser source in OFDR, spectroscopy and Lidar systems.

REFERENCES

[1] H. Al-Taiy, N. Wenzel, S. Preußler, J. Klinger, and T. Schneider, "Ultra-narrow linewidth, stable and tunable laser source for optical communication systems and spectroscopy," *Opt. Lett.*, vol. 39, no. 20, pp. 5826–5829, 2014, doi: 10.1364/OL.39.005826.

[2] N. Cézard *et al.*, "Performance assessment of a coherent DIAL-Doppler fiber LiDAR at 1645 nm for remote sensing of methane and wind," *Opt. Exp.*, vol. 28, pp. 22345–22357, 2020, doi: 10.1364/OE.394553.

[3] J. Qin *et al.*, "Ultra-long range optical frequency domain reflectometry using a coherence-enhanced highly linear frequency-swept fiber laser source," *Opt. Exp.*, vol. 27, pp. 22345–22357, 2019, doi: 10.1364/OE.27.019359.

[4] H. Katori, "Optical lattice clocks and quantum metrology," *Nature Photon.*, vol. 5, no. 4, pp. 203–210, 2011, doi: 10.1038/nphoton.2011.45.

[5] C. W. Chou, R. B. Hume, R. Rosenband, and R. J. Wineland, "Optical clocks and relativity," *Science*, vol. 329, no. 5999, pp. 1630–1632, 2010, doi: 10.1126/science.1192720.

[6] C. Yang *et al.*, "15 W high OSNR kHz-linewidth linearly-polarized all-fiber single-frequency MOPA at 1.6 μm," *Opt. Exp.*, vol. 26, no. 10, pp. 12863–12869, 2018, doi: 10.1364/OE.26.012863.

[7] Y. Wang *et al.*, "Single-frequency DBR Nd-doped fiber laser at 1120 nm with a narrow linewidth and low threshold," *Opt. Lett.*, vol. 45, no. 8, pp. 2263–2266, 2020, doi: 10.1364/OL.386477.

[8] R. A. Pérez-Herrera, L. Rodríguez-Cobo, M. A. Quintela, J. M. López Higuera, and M. López-Amo, "Single-longitudinal-mode dual wavelength-switchable fiber laser based on superposed fiber Bragg gratings," *IEEE Photon. J.*, vol. 7, no. 2, Apr. 2015, Art. no. 7101307, doi: 10.1109/JPHOT.2015.2419077.

[9] C. H. Yeh, Y. Hsu, and C. W. Chow, "Utilizing a silicon-photonic micro-ring-resonator and multi-ring scheme for wavelength-switchable erbium fiber laser in single-longitudinal-mode," *Laser Phys. Lett.*, vol. 13, no. 6, 2016, Art. no. 065103, doi: 10.1088/1612-2011/13/6/065103.

[10] A. A. Jasim, M. Dernaika, S. W. Harun, and H. Ahmad, "A switchable figure eight erbium-doped fiber laser based on inter-modal beating by means of non-adiabatic microfiber," *J. Lightw. Technol.*, vol. 33, no. 2, pp. 528–534, 2015, doi: 10.1109/JLT.2015.2390654.

[11] B. Yin, S. Feng, Z. Liu, Y. Bai, and S. Jian, "Tunable and switchable dual-wavelength single polarization narrow linewidth SLM erbium-doped fiber laser based on a PM-CMFBG filter," *Opt. Exp.*, vol. 22, no. 19, pp. 22528–22533, 2014, doi: 10.1364/OE.22.022528.

[12] K. K. Qureshi, "Switchable dual-wavelength fiber ring laser featuring twin-core photonic crystal fiber-based filter," *Chin. Opt. Lett.*, vol. 12, no. 2, 2014, Art. no. 020605, doi: 10.3788/COL201412.020605.

[13] Z. Cao *et al.*, "Switchable dual-wavelength erbium-doped fiber ring laser with tunable wavelength spacing based on a compact fiber filter," *Opt. Laser Technol.*, vol. 56, pp. 137–141, 2014, doi: 10.1016/j.optlastec.2013.07.021.

[14] W. Zheng, S. Ruan, M. Zhang, W. Liu, Y. Zhang, and X. Yang, "Switchable multi-wavelength erbium-doped photonic crystal fiber laser based on nonlinear polarization rotation," *Opt. Laser Technol.*, vol. 50, pp. 145–149, 2013, doi: 10.1016/j.optlastec.2013.01.022.

[15] L. Wei and J. W. Y. Lit, "Compound ring resonator with double couplers," *Opt. Commun.*, vol. 186, no. 4, pp. 283–290, 2000, doi: 10.1016/S0030-4018(00)01083-X.

[16] S. Feng, Q. Mao, Y. Tian, Y. Ma, W. Li, and L. Wei, "Widely tunable single longitudinal mode fiber laser with cascaded fiber-ring secondary cavity," *IEEE Photon. Technol. Lett.*, vol. 25, no. 4, pp. 323–326, Feb. 2013, doi: 10.1109/LPT.2012.2235141.

[17] T. Feng, F. Yan, S. Liu, Y. Bai, W. Peng, and S. Tan, "Switchable and tunable dual-wavelength single-longitudinal-mode erbium-doped fiber laser with special subring-cavity and superimposed fiber Bragg gratings," *Laser Phys. Lett.*, vol. 11, no. 12, 2014, Art. no. 125106, doi: 10.1088/1612-2011/11/12/125106.

[18] T. Feng, D. Ding, Z. Zhao, H. Su, F. Yan, and X. S. Yao, "Switchable 10 nm-spaced dual-wavelength SLM fiber laser with sub-kHz linewidth and high OSNR using a novel multiple-ring configuration," *Laser Phys. Lett.*, vol. 13, no. 10, 2016, Art. no. 105104, doi: 10.1088/1612-2011/13/10/105104.

[19] T. Feng, D. Ding, F. Yan, Z. Zhao, H. Su, and X. S. Yao, "Widely tunable single-/dual-wavelength fiber lasers with ultra-narrow linewidth and high OSNR using high quality passive subring cavity and novel tuning method," *Opt. Exp.*, vol. 24, no. 17, pp. 19760–19768, 2016, doi: 10.1364/OE.24.019760.

[20] T. Feng, D. Ding, P. Liu, H. Su, and X. S. Yao, "Widely tunable/wavelength-swept SLM fiber laser with ultra-narrow linewidth and ultra-high OSNR," *Optoelectron. Lett.*, vol. 12, no. 6, pp. 0433–0436, 2016, doi: 10.1007/s11801-016-6194-z.

[21] T. Feng, M. Wang, X. Wang, F. Yan, Y. Suo, and S. Yao, "Switchable 0.612 nm-spaced dual-wavelength fiber laser with sub-kHz linewidth, ultra-high OSNR, ultra-low RIN and orthogonal polarization outputs," *J. Lightw. Technol.*, vol. 37, pp. 3173–3182, 2019, doi: 10.1109/JLT.2019.2912432.

[22] T. Feng *et al.*, "Four-wavelength-switchable SLM fiber laser with sub-kHz linewidth using superimposed high-birefringence FBG and dual-coupler ring based compound-cavity filter," *Opt. Exp.*, vol. 27, no. 25, pp. 36662–36679, 2019, doi: 10.1364/OE.27.036662.

[23] T. Feng *et al.*, "Wavelength-switchable ultra-narrow linewidth fiber laser enabled by a figure-8 compound-ring-cavity filter and a polarization-managed four-channel filter," *Opt. Exp.*, vol. 29, no. 20, pp. 31179–31200, 2021, doi: 10.1364/OE.439732.

[24] C. Goh, S. Set, K. Kikuchi, M. Mokhtar, S. Butler, and M. Ibsen, "Greater than 90 nm continuously wavelength-tunable fibre Bragg gratings," in *Proc. Opt. Fiber Commun. Conf.*, vol. 2, Atlanta, GA, 2003, pp. 643–644, doi: 10.1109/OFC.2003.316196.

[25] Y. W. Song, S. A. Havstad, D. Starodubov, Y. Xie, and J. Feinberg, "40-nm-wide tunable fiber ring laser with single-mode operation using a highly stretchable FBG," *IEEE Photon. Technol. Lett.*, vol. 13, no. 11, pp. 1167–1169, Nov. 2001, doi: 10.1109/68.959352.

[26] S. H. Yun, C. Boudoux, G. J. Tearney, and B. E. Bouma, "High-speed wavelength-swept semiconductor laser with a polygon-scanner-based wavelength filter," *Opt. Lett.*, vol. 28, no. 20, pp. 1981–1983, 2003, doi: 10.1364/OL.28.001981.

[27] S. H. Yun, D. J. Richardson, and D. O. Culverhouse, "Wavelength-swept fiber laser with frequency shifted feedback and resonantly swept intracavity acoustooptic tunable filter," *IEEE J. Sel. Topics Quantum*, vol. 3, no. 4, pp. 1087–1096, Aug. 1997, doi: 10.1109/2944.649546.

[28] M. A. Choma, K. Hsu, and J. A. Izatt, "Swept source optical coherence tomography using an all-fiber 1300-nm ring laser source," (in English), *J. Biomed. Opt.*, vol. 10, no. 4, 2005, Art. no. 044009, doi: 10.1117/1.1961474.

[29] R. Huber, D. C. Adler, and J. G. Fujimoto, "Buffered Fourier domain mode locking: Unidirectional swept laser sources for optical coherence tomography imaging at 370,000 lines/s," *Opt. Lett.*, vol. 31, no. 20, pp. 2975–2977, 2006, doi: 10.1364/OL.31.002975.

[30] L. N. Binh, S. F. Luk, and N. Q. Ngo, "Amplified double-coupler double-ring optical resonators with negative optical gain," *Appl. Opt.*, vol. 34, no. 27, pp. 6086–6094, 1995, doi: 10.1364/AO.34.006086.

[31] S. Mason, "Feedback theory-further properties of signal flow graphs," *Proc. IRE*, vol. 44, pp. 920–926, 1956, doi: 10.1109/JRPROC.1956.275147.

[32] I. S. Amiri, S. Soltanmohammadi, A. Shahidinejad, and J. Ali, "Optical quantum transmitter with finesse of 30 at 800-nm central wavelength using microring resonators," *Opt. Quantum Electron.*, vol. 45, no. 10, pp. 1095–1105, 2013, doi: 10.1007/s11082-013-9726-9.

[33] I. S. Amiri, S. E. Alavi, M. R. Soltanian, N. Fisal, A. S. Supa'at, and H. Ahmad, "Increment of access points in integrated system of wavelength division multiplexed passive optical network radio over fiber," *Sci. Rep.*, vol. 5, 2015, Art. no. 11897, doi: 10.1038/srep11897.

[34] F. Sanchez, "Matrix algebra for all-fiber optical resonators," *J. Lightw. Technol.*, vol. 9, pp. 838–844, 1991, doi: 10.1109/50.85783.

[35] P. Urquhart, "Compound optical-fiber-based resonators," *J. Opt. Soc. Amer. A*, vol. 5, pp. 803–812, Jun. 1988, doi: 10.1364/JOSAA.5.000803.

[36] J. O. Gerguis, Y. M. Sabry, and D. Khalil, "Capturing the instantaneous spectral response of a MEMS swept laser source using a quasi-static tunable filter," *IEEE J. Sel. Topics Quantum*, vol. 25, no. 6, Nov./Dec. 2019, Art no. 2800108, doi: 10.1109/JSTQE.2019.2893759.

[37] B. R. Biedermann, W. Wieser, C. M. Eigenwillig, T. Klein, and R. Huber, "Direct measurement of the instantaneous linewidth of rapidly wavelength-swept lasers," *Opt. Lett.*, vol. 35, no. 22, pp. 3733–3735, 2010, doi: 10.1364/OL.35.003733.

[38] C. Zhang, J. Xu, P. C. Chui, and K. K. Wong, "Parametric spectro-temporal analyzer (PASTA) for real-time optical spectrum observation," *Sci. Rep.*, vol. 3, 2013, Art. no. 2064, doi: 10.1038/srep02064.

[39] X. S. Yao, B. Zhang, X. Chen, and A. E. Willner, "Real-time optical spectrum analysis of a light source using a polarimeter," *Opt. Exp.*, vol. 16, no. 22, pp. 17854–17863, 2008, doi: 10.1364/OE.16.017854.

[40] S. Mo *et al.*, "820 Hz linewidth short-linear-cavity single-frequency fiber laser at 1.5 μm," *Laser Phys. Lett.*, vol. 11, 2014, Art. no. 035101, doi: 10.1088/1612-2011/11/3/035101.